Journal of Hazardous Materials 181 (2010) 722–728

Contents lists available at ScienceDirect

Journal of Hazardous Materials

journal homepage: www.elsevier.com/locate/jhazmat

Nitrate storage behavior of $Ba/MnO_x–CeO_2$ catalyst and its activity for soot oxidation with heat transfer limitations

Xiaodong Wu*, Shuang Liu, Fan Lin, Duan Weng

State Key Laboratory of New Ceramics & Fine Process, Department of Materials Science and Engineering, Tsinghua University, Beijing 100084, China

ARTICLE INFO

Article history:
Received 24 February 2010
Received in revised form 19 April 2010
Accepted 17 May 2010
Available online 9 June 2010

Keywords:
MnOx–CeO2 mixed oxides
Barium
Soot oxidation
Nitrate

ABSTRACT

A BaMnCe ternary catalyst was prepared by impregnating barium acetate on $MnO_x–CeO_2$ mixed oxides, with the monoxide supported catalysts and the solid solution support as references. The activities of the catalysts for soot oxidation were evaluated in the presence of NO under an energy transference controlled regime. BaMnCe presented the lowest maximal soot oxidation rate temperature at 393 °C among the catalysts investigated. Although BaMnCe experienced a loss in the specific surface area and low–temperature redox property due to blocking of the support pores by barium carbonate, its superior soot oxidation activity highlighted the importance of relatively stable bidentate/monodentate nitrates coordinated to Mn^{x+} and Ce^{x+} sites and more stable ionic barium nitrate. About half of the nitrates stored on this catalyst decomposed within the temperature interval of 350–450 °C, and the ignition temperature of soot decreased significantly with involvement of the nitrates or NO_2 released.

1. Introduction

The removal of soot in diesel exhaust is a topic of ongoing researches due to the environmental and health impacts of these carbon nanoparticles [1]. To develop suitable catalysts capable of promoting soot oxidation by NO_x is an efficient way for removal of soot at relative low temperatures. Among the catalysts investigated, novel metals such as platinum are one of the most active kinds as they can effectively catalyze oxidation of NO to NO_2 [2,3].

However, the soot oxidation rate would be limited by the reduced NO_x concentration in exhaust gas from modern engines. The NO_x storage feature of alkali and alkaline earth metals can provide additional desorbed NO_2 at moderate temperatures and thus make them a promising component in soot oxidation catalysts. Potassium has been widely introduced to catalysts to reduce the maximal soot oxidation temperature (T_m) to 350 °C or even lower owing to the high NO_x storage capacity and low molten point of potassium salts [4–10]. Recently, barium has received more and more attention in simultaneous removal of soot and NO_x by Pt–containing NSR (NO_x storage reduction) catalysts [11,12] and catalytic oxidation of soot by potassium–copromoted catalysts ($Ba,K/CeO_2$ [13,14], $Co,Ba,K/CeO_2$ [15], $Co,Ba,K/ZrO_2$ [16,17] and $Co,Ba,K/Al_2O_3$ [18]).

The strong oxidative property of manganese oxides in combination with the oxygen storage property of ceria makes $MnO_x–CeO_2$ mixed oxides catalyst as one group of cheap and efficient candidate catalysts for soot oxidation, which can be traced to its ability to store NO_x at low temperatures in form of nitrates followed by a release of NO_2 as a strong oxidizing agent at high temperatures [19]. The addition of Cs to $MnO_x–CeO_2$ has been found to further promote the soot oxidation, and the adsorbed nitrate species are considered to act as an oxidizing agent to promote soot ignition [20].

The exothermic oxidation of soot can damage the cordierite filters used in virtually heavy–duty continuously regenerating trap [21,22]. The occurrence of this uncontrolled regeneration of soot depends upon the technique being used. The reaction mechanism is very complex and that there are many factors to be taken into account, such as low catalyst/soot weight ratio, low heat conductivity and low oxygen pressure [7,23,24]. In the present work, Ba was impregnated on the $MnO_x–CeO_2$, MnO_x and CeO_2 supports to modify the NO_x storage behavior of the catalysts. The obtained catalysts were characterized by XRD, BET, H_2–TPR, NO_x–TPD and *in situ* DRIFTS. A reaction runaway was likely to take place when the heat generation rate was above a threshold for the undiluted soot–catalyst system. The objective was to analyze the contribution of the stored nitrates on the catalysts to soot oxidation with heat transfer limitations.

2. Experimental

2.1. Catalyst preparation

$MnO_x–CeO_2$ mixed oxides (MnCe) were prepared by a sol–gel method. The nitrate precursors $Ce(NO_3)_3·6H_2O$ (99.0 wt.%, Beijing Yili) and $Mn(NO_3)_2$ (50 wt.% water solution, Yili) were mixed in

* Corresponding author. Tel.: +86 10 62792375; fax: +86 10 62792375.
E-mail address: wuxiaodong@tsinghua.edu.cn (X. Wu).

0304-3894/$ – see front matter © 2010 Elsevier B.V. All rights reserved.
doi:10.1016/j.jhazmat.2010.05.072

deionized water according to the molar ratio of Mn:Ce = 1:9. The citric acid was added as the complexing agent with a 2:1 ratio of the acid to metal ions including Ce^{3+} and Mn^{2+}. Polyglycol was followed with the weight of 10% citric acid added. The solution was sufficiently stirred and heated at 80 °C till a gel was formed. The gel was dried at 110 °C overnight followed by decomposition at 300 °C for 1 h and calcination at 500 °C for 3 h. The monoxides MnO_x and CeO_2 were prepared by a similar method as the reference supports.

The acetate $Ba(Ac)_2$ was loaded on MnO_x–CeO_2 mixed oxides by a wetness impregnation method according to the ratio of $BaO/(BaO + Mn_2O_3 + CeO_2)$ = 10 wt.%. The mixture was dried at 110 °C for 2 h and calcined at 550 °C for 1 h. The resulting catalyst was referred to as BaMnCe. The monoxide supported catalysts BaCe and BaMn were prepared by impregnating barium acetate on CeO_2 and MnO_x, respectively, with a given BaO content of 10 wt.%.

2.2. Catalyst characterization

The powder X–ray diffraction (XRD) patterns were determined by a Japan Science D/max–RB diffractometer employing Cu Kα radiation (λ=0.15418 nm). The X–ray tube was operated at 40 kV and 120 mA. The X–ray diffractograms were recorded at 0.02° intervals in the range of $20° \le 2\theta \le 80°$ with a scanning velocity of 6°/min. The lattice constants and mean crystallite sizes of ceria in the samples were calculated from Cohen's method and Debye–Scherrer equation, respectively.

The specific surface areas of the samples were measured using the N_2 adsorption at–196 °C by the four–point Brunauer–Emmett–Teller (BET) method using an automatic surface analyzer (F–Sorb 3400, Gold APP Instrument). The samples were degassed in flowing N_2 at 200 °C for 2 h.

The H_2 temperature–programmed reduction (TPR) tests were carried out in a fixed–bed reactor with the effluent gases monitored by a mass spectrometer (OmniStar TM). Twenty five milligrams of the sample was sandwiched by quartz wool and placed in a tubular quartz reactor. The reactor temperature was raised up to 900 °C at a heating rate of 10 °C/min in 5% H_2/He (50 ml/min).

The diffuse reflectance infrared Fourier transformed spectra (DRIFTS) were recorded on a Nicolet 6700 spectrometer. The sample powders were purged *in situ* in a N_2 stream (100 ml/min) at 450 °C for 30 min. The background spectrum was taken from 50 to 450 °C at an interval of 50 °C. After then, a gas mixture of 1000 ppm NO/10% O_2/N_2 was fed at a flow rate of 100 ml/min. The spectra were determined by accumulating 100 scans at a resolution of 4 cm^{-1} as a function of temperature at a heating rate of 10 °C/min.

The NO_x temperature–programmed desorption (TPD) tests were performed in a fixed–bed reactor with the emission monitored by an infrared spectrometer (Thermo Nicolet 380). Prior to the test, the sample powders were exposed in 1000 ppm NO/10% O_2/N_2 (500 ml/min) at 350 °C for 30 min, cooled down to room temperature (RT) in the same atmosphere and flushed by N_2 (100 ml/min) for 10 min. After then, the NO and NO_2 desorption profiles were obtained by ramping the reactor from RT to 600 °C at a heating rate of 10 °C/min in a N_2 stream. The infra-red bands at 1855.1-1851.2 and 1599.8-1597.4 cm^{-1} were applied for detecting NO and NO_2, respectively.

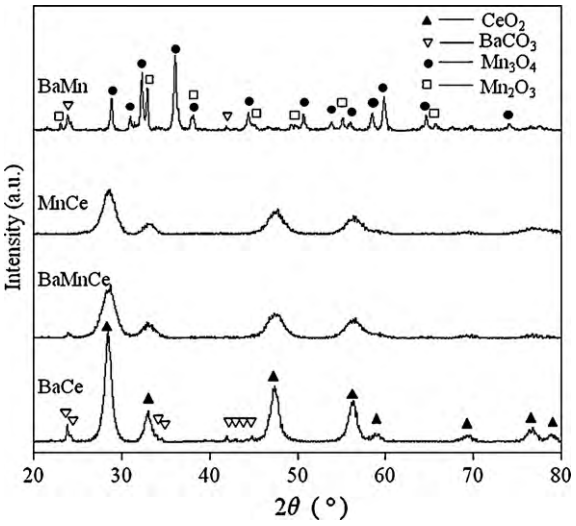

Fig. 1. XRD patterns of the samples.

2.3. Catalyst activity measurement

Printex–U (Degussa) was used as a model soot. Its particle size was 25 nm and the specific surface area was 100 m^2/g. The activities of the catalysts for soot oxidation were evaluated in a temperature–programmed oxidation (TPO) reaction apparatus. Ten milligrams of soot and one hundred milligrams of catalyst powders were mixed by a spatula for 2 min for "loose contact" conditions. The catalyst–soot mixture was placed in a tubular quartz reactor, and the oxidation test was carried out from RT to 600 °C at a heating rate of 15 °C/min. The inlet gas mixture was 1000 ppm NO/10% O_2/N_2 or 10% O_2/N_2 (500 ml/min). The outlet CO_2, CO, NO and O_2 concentrations were determined online by a five–component analyzer FGA4015. The downstream $CO_2/(CO_2 + CO)$ ratio during soot oxidation was defined as the selectivity to CO_2.

3. Results

3.1. XRD and BET

The powder XRD patterns of the samples are shown in Fig. 1. The structural properties of the samples based on the XRD data and BET method are listed in Table 1. Typical diffraction peaks of cubic ceria are obviously broadened on MnCe and BaMnCe in comparison with BaCe. Barium exists in the form of the orthorhombic carbonate on the Ba–containing samples. The weakened intensities of $BaCO_3$ peaks on BaMnCe indicate a low crystallization degree of the carbonate crystallites on the mixed oxides support. The Mn species in BaMn exist in the form of cubic Mn_2O_3 and tetragonal Mn_3O_4 in +3 and +2 oxidation states. However, no diffraction peaks of manganese oxides are detected in the patterns of MnCe and BaMnCe. As listed in Table 1, the mean lattice constants of ceria in MnCe and BaMnCe are smaller than that in BaCe, indicating the incorporation of Mn^{x+} cations into the ceria lattice due to the smaller ionic radii of Mn^{3+} (0.065 nm) and Mn^{2+} (0.083 nm) than those of Ce^{4+}

Table 1
Structural properties of the samples.

Catalyst	Lattice constant of CeO_2 (nm)	Crystallite size of CeO_2 (nm)	S_{BET} (m^2/g)
BaCe	0.5416 ± 0.0003	8.2 ± 0.1	58
BaMnCe	0.5407 ± 0.0006	4.4 ± 0.1	81
MnCe	0.5406 ± 0.0004	4.4 ± 0.1	153
BaMn	–	–	12

(0.097 nm) and Ce^{3+} (0.114 nm). No nitrates seem to residue in the samples after calcination since no NO_x species are released by heating the catalysts in N_2 up to 650 °C (not shown). The feasibility of decomposition of the related nitrates at 500 °C is confirmed by the NO_x-TPD results in section 3.4.

The formation of MnO_x–CeO_2 solid solutions facilitates the MnCe sample to present a specific surface area larger than 150 m^2/g since the doped manganese oxide inhibits the sintering of ceria as reflected by the crystallite size of CeO_2. Although the BET surface area of BaMnCe decreases to some extent due to blocking of the support pores by loading the barium salt, it is still larger than those of the monoxide supported catalysts.

3.2. H_2–TPR

The H_2–TPR tests were applied to estimate the reducibility of the catalysts since the oxidation of soot involves chemisorbed oxygen and especially lattice oxygen at high temperatures, and the results are shown in Fig. 2. Several reduction peaks are found at 217, 285 and 362 °C on MnCe, which result from two types of oxygen species. One is the surface chemisorbed oxygen associated with the low-temperature peak and the other is the lattice oxygen from the reduction of $Mn_2O_3 \rightarrow Mn_3O_4$ and $Mn_3O_4 \rightarrow MnO$ strongly interacted with ceria at the two high–temperature peaks [25]. After introducing Ba to the mixed oxides, the low-temperature peak shifts to 240 °C and decreases in intensity. The two high-temperature peaks shift to 325 and 412 °C, respectively. These shifts

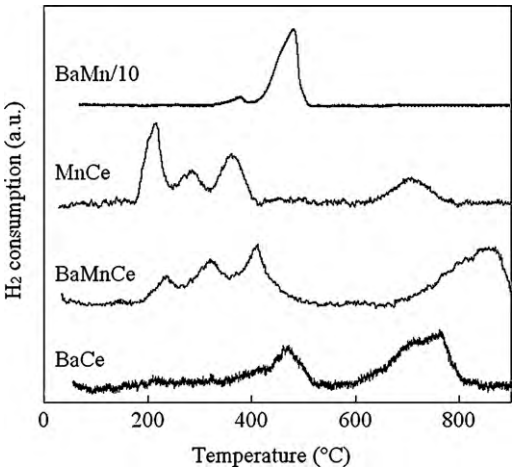

Fig. 2. H_2–TPR profiles of the catalysts.

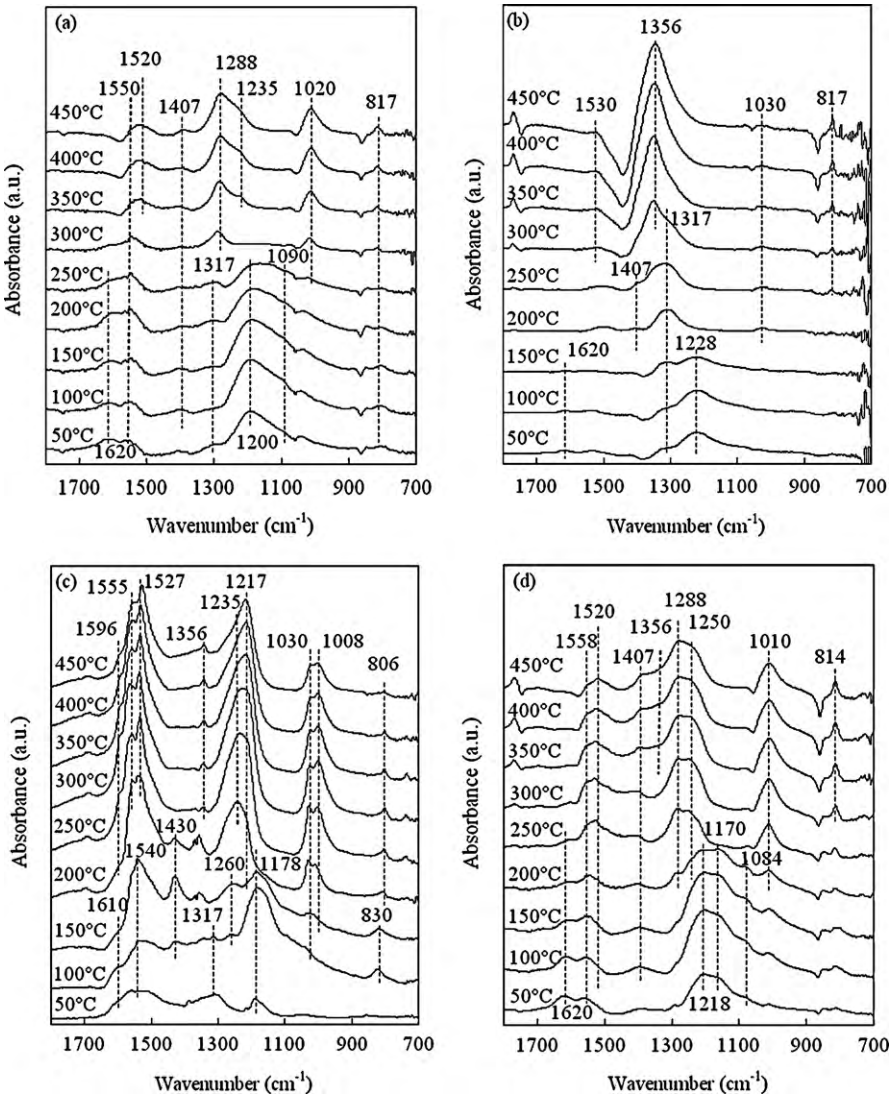

Fig. 3. DFIRT spectra obtained on (a) BaCe, (b) BaMn, (c) MnCe and (d) BaMnCe in $NO + O_2$.

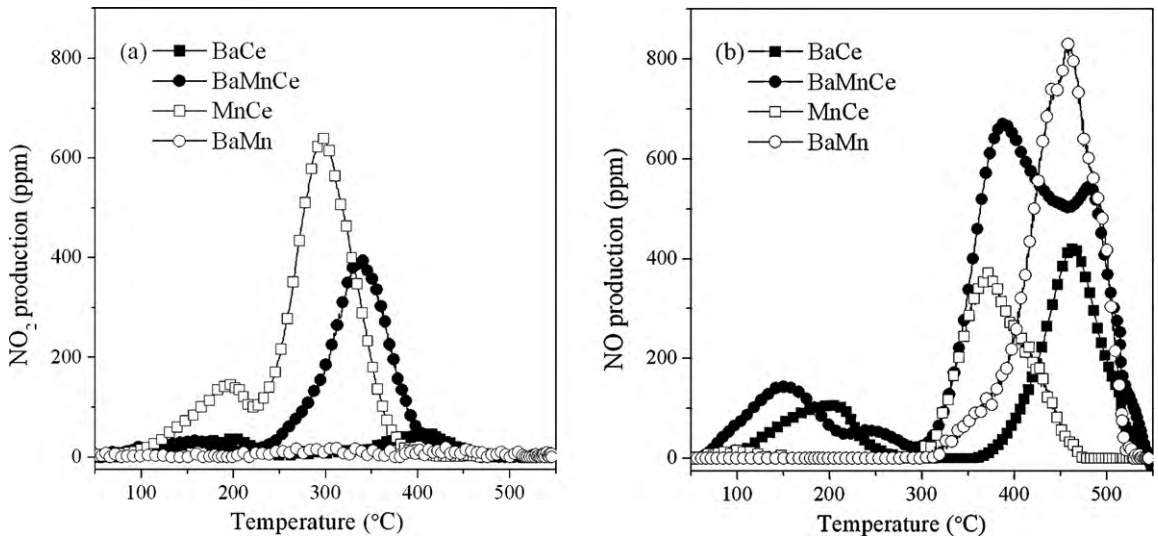

Fig. 4. (a) NO_2–and (b) NO–TPD profiles of the catalysts.

to higher temperatures by 20–50 °C may be caused by the partial coverage with barium which impedes the reduction of surface and lattice oxygens from MnO_x–CeO_2 mixed oxides as well as the reduced surface area. The reduction of lattice oxygen from CeO_2 also seems to be retarded by the barium coverage with a shift of the peak temperature from 710 to 860 °C.

A distinct peak centered at 484 °C is observed on BaMn attributed to two overlapped strong reduction peaks of $Mn_2O_3 \rightarrow Mn_3O_4$ and $Mn_3O_4 \rightarrow MnO$. Its peak intensity is about 10 times of those obtained on the other samples owing to the dominant content of manganese. The reduction of amorphous MnO_2 in trace to Mn_2O_3 may be responsible for the small peak centered at 295 °C [26]. Two reduction peaks are observed on BaCe at 473 and 740 °C, which are ascribed to the reduction of surface and bulk oxygen from ceria, respectively.

3.3. *In situ DRIFTS*

The DRIFT spectra of adsorbed species on the catalysts arising from contact of $NO + O_2$ were recorded to gain insight into the types of stored NO_x species as a function of temperature, and the results are shown in Fig. 3. At low temperatures (< 250 °C), the adsorbed species on BaCe in Fig. 3a are mainly nitrites (1200 and 1090 cm^{-1}) accompanied by some weakly adsorbed NO_2 (1620 cm^{-1}) [27,28]. The nitrite bands diminish from 100 °C and are completely replaced by those assigned to the bidentate nitrate (1550, 1288 and 1020 cm^{-1}) and monodentate nitrate (1520 and 1235 cm^{-1}) mostly coordinated to Ce^{x+} sites at 300 °C. The nitrate bands increase in intensity with temperature. Bands at 1407 and 1317 cm^{-1} are associated to nitro compounds. The minus bands at 1063 and 870 cm^{-1} are ascribed to the decomposition of $BaCO_3$ [13]. It is a pity that the upper limit of permitted temperature in this case is 450 °C, although the band at 817 cm^{-1} may imply the formation of ionic barium nitrate at high temperatures.

Comparatively, the adsorption of nitrites (1228 cm^{-1}) and NO_2 (1620 cm^{-1}) at low temperatures is much less pronounced on BaMn in Fig. 3b. The main adsorbed species turn to be nitro compounds (1407 and 1317 cm^{-1}) at 200–250 °C. The ionic nitrate (1356 and 817 cm^{-1}) becomes predominant at the temperatures above 300 °C due to the strong oxidation ability of manganese oxide and high basicity of barium salt. The simultaneous appearance of minus bands (1450, 1063 and 860 cm^{-1}) indicates the transformation of barium carbonate to ionic nitrates.

The adsorption of NO_x is quite strong on MnCe as shown in Fig. 3c. The low–temperature adsorbed species are complex, including weakly adsorbed NO_2 (1610 cm^{-1}), nitrites (1178 cm^{-1}), nitro–nitrite (1540 cm^{-1}) and nitro compounds (1430, 1260 and 1317 cm^{-1}). These less stable NO_x–derived species are quickly transformed to the nitrates species including monodentate nitrates (1527, 1235 and 1008 cm^{-1}), bidentate nitrates (1555, 1288 and 1030 cm^{-1}) and bridging nitrates (1596, 1234 and 1008 cm^{-1}) from 200 °C. These nitrate bands reach the maximum at 300 °C. The bands ascribed to stable ionic nitrates (1356 and 806 cm^{-1}) are quite weak since the catalyst does not contain any high basic components such as barium.

By introduction of barium carbonate onto MnO_x–CeO_2 mixed oxides, the nitrite bands (1218, 1170 and 1084 cm^{-1}) reach the maximum at 100 °C in Fig. 3d. When the temperature rises to 250 °C, the nitrite bands are replaced by those assigned to bidentate nitrates (1558, 1288 and 1010 cm^{-1}) and monodentate nitrates (1520, 1250 and 1010 cm^{-1}). Therefore, it is deduced that the temperature for transformation of nitrites to nitrates on MnO_x–CeO_2 mixed oxides is elevated by loading of barium. In addition to the bidentate/monodentate nitrates, the stable ionic nitrates (1356 and 814 cm^{-1}) start to form from 300 °C and keep increasing with temperature. The minus bands at 1456, 1065 and 862 cm^{-1} are also observed due to the transformation of barium carbonate to the nitrate.

3.4. *NO_x–TPD*

To study the NO_x storage capacities of the catalysts, the NO_x–TPD tests were carried out in N_2 after adsorption in $NO + O_2$ at 350 °C. As shown in Fig. 4a, two NO_2 desorption peaks at 195 and 295 °C are observed on MnCe ascribed to desorption of weakly adsorbed NO_2 and decomposition of nitrates, respectively. Considering that NO oxidation is kinetically favored at the adsorption temperature, the most stable ad–NO_x species, i.e. nitrates, are predominant as indicated by the DRIFT spectra. Thus, the NO desorption centered at 370 °C in Fig. 4b is likely to arise from the thermodynamic–driven decomposition of NO_2 and/or NO_2 dissociation on reducible metal sites under N_2 [29].

The amount and temperature of NO_x desorption on BaMnCe are quite different from those on MnCe. The NO_2 peak temperature shifts from 295 to 340 °C. A low–temperature NO peak appears at 150 °C ascribed to desorption of weakly adsorbed NO

and/or decomposition of surface nitrites. A bimodal shape of the nitrate–derived NO desorption is observed with one peak at 385 °C and the other at 480 °C. The first high–temperature NO peak is ascribed to the decomposition/dissociation of NO_2 arising from decomposition of bidentate/monodentate nitrates mainly coordinated to Mn^{x+} and Ce^{x+} sites since it correlates well with that on MnCe. The latter high–temperature NO peak is ascribed to the decomposition/dissociation of NO_2 deriving from decomposition of barium nitrate.

Almost no NO_2 is desorbed from BaMn in Fig. 4a, while two minor NO_2 peaks are observed at 177 and 400 °C on BaCe ascribed to decomposition of weakly adsorbed NO_2 and decomposition of bidentate/monodentate nitrates, respectively. The low–temperature NO peak at 200 °C on BaCe is ascribed to desorption of weakly adsorbed NO and/or decomposition of nitrites, which is not observed on BaMn. A distinct NO desorption peak associated with the decomposition/dissociation of the nitrate–derived NO_2 appears at 460 °C on two monoxide supported catalysts. The above results are in good accordance with the *in situ* DRIFT spectra in Fig. 3 except those obtained on BaCe. The adsorbed species on BaCe are mainly bidentate/monodentate nitrates coordinated to Ce^{x+} sites at 300–450 °C according to the DRIFT spectra, while the majority of NO_x desorbed in the TPD test is suggested to originate from the decomposition of ionic barium nitrate. It probably results from the transformation of bidendtate/monodentate nitrates to ionic nitrate on BaCe with exposure to NO + O_2 at 350 °C for 30 min.

The total amount of NO_x (NO + NO_2) desorbed, which was estimated from the desorption profiles, is an effective indicator of NO_x storage capacity of catalysts. The calculated value is 0.31, 0.39, 0.44 and0.97 mmol/g cat. for BaCe, MnCe, BaMn and BaMnCe, respectively. Thus, the efficiency of barium utilization for NO_x storage is 38%, 29% and 24% on the MnO_x, MnO_x–CeO_2 and CeO_2 support, respectively, indicating that the efficiency of NO_x storage is related not only to the dispersion of the NO_x storage component but also to the oxidation ability of the support.

3.5. Soot–TPO

The activities of the catalysts were evaluated by soot–TPO tests in the presence of 1000 ppm NO and 10% O_2. The tests were repeated for three times and the same trend of activities of the catalysts was obtained. The selectivity to CO_2 in the products of soot oxidation with the catalysts follows the order of BaMn (99%) = BaMnCe (99%) > MnCe (95%) > BaCe (92%), indicating the partial oxidation of soot is not significant. Thus, Fig. 5 only shows the evolutions of CO_2 during the TPO tests for clarity. BaMnCe exhibits the lowest T_m at 393 °C among the catalysts investigated. The T_m of MnCe, BaMn and BaCe is located at 410, 400 and 478 °C, respectively. Comparatively, the T_m value obtained in O_2 is 537, 491, 547 and 540 °C for BaMnCe, MnCe, BaMn and BaCe, respectively. The different sequence of activity obtained in NO-containing and NO-free atmospheres demonstrates the predominance of BaMnCe in NO_x–assisted soot oxidation. It should be noted that a reaction runaway may take place since no diluents were applied to the soot-catalyst mixture. The obtained sharp TPO peaks suggest that the soot catalytic oxidation occurs under an energy transference controlled regime in this work.

The evolutions of NO during the soot–TPO tests were also recorded and the results are shown in Fig. 6. An obvious slip of the NO concentration is observed for BaMn at low temperatures centered at 330 °C due to NO oxidation to NO_2, which can be attributed to the strong oxidation ability of manganese oxides as the dominant component in this catalyst. Contrarily, the decrease of NO is not obvious on BaCe because of the mild oxidation ability of ceria which is further weakened by the coverage with barium carbonate. The NO drops on MnO_x–CeO_2 mixed oxides and the corresponding

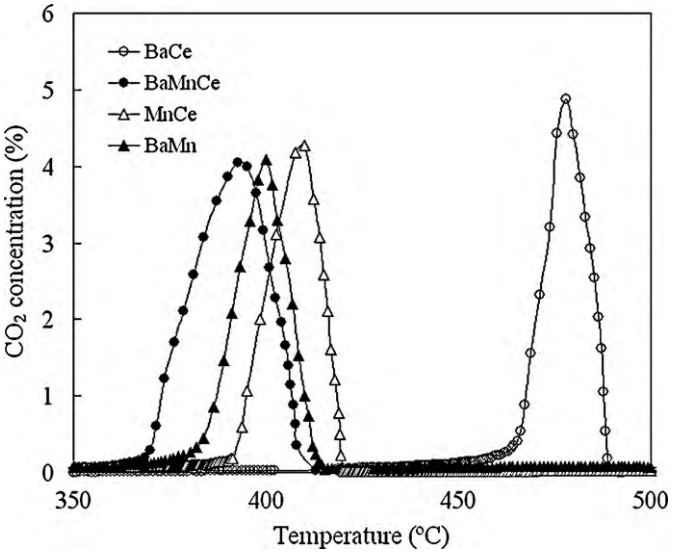

Fig. 5. TPO profiles of the soot–catalyst mixtures obtained in NO + O_2 under loose contact conditions.

Ba-supported catalyst are between these two cases. All the catalysts show a NO rise simultaneously with the ignition of soot. The NO peak intensity follows the order of BaMnCe > BaMn > MnCe > BaCe. This NO production is thought to initially arise from the reduction of the nitrate–and NO–derived NO_2 by soot. The exothermic soot oxidation reaction, in turn, accelerates the further decomposition of nitrates to produce more NO_x with heat transfer limitations. Ultimately the extensive oxidation of soot by O_2 is initiated. Both these contributions can be considered as NO_x–assisted soot oxidation. It should be demonstrated that oxygen is the major oxidant during the whole process.

4. Discussion

4.1. Effect of nitrate decomposition temperature

According to the above results, it is important for NO_x desorption to occur within a required temperature interval in which soot oxidation can be promoted by NO_2. M. Makkee's group got an optimal interval for NO_x release between 350 and 450 °C based on

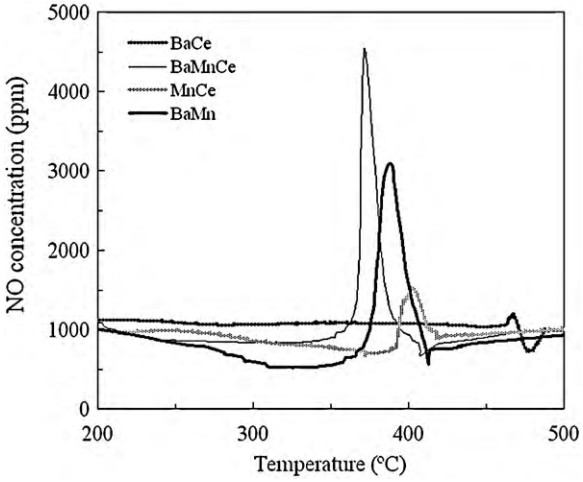

Fig. 6. Evolutions of the downstream NO during the soot–TPO tests with the catalysts.

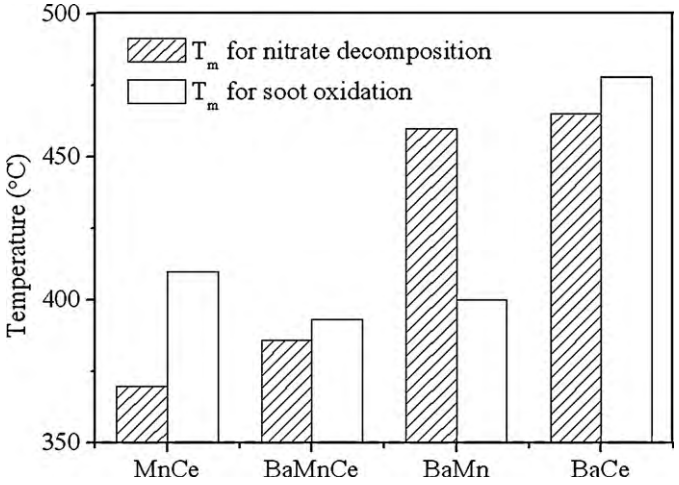

Fig. 7. Relationship between the T_m values for nitrate decomposition and those for soot oxidation.

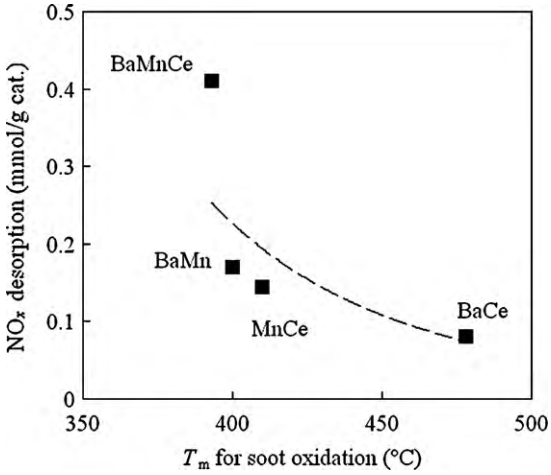

Fig. 8. Relationship between the amount of nitrate decomposition and T_m for soot oxidation.

alkali–earth oxides supported on Al_2O_3 [30]. A similar suggestion can be attained in this work.

It is known from the NO_x–TPD profiles and *in situ* DRIFT spectra that the NO desorbed above 300 °C arises from the thermodynamic–driven decomposition of nitrate–derived NO_2. Therefore, it is plausible to refer to the high–temperature NO desorption peak temperature as the maximal nitrate decomposition rate temperature (T_m for nitrate decomposition). For simplicity, only the first high–temperature NO desorption peak was taken into account for BaMnCe. Fig. 7 compares the T_m values for nitrate decomposition and those for soot oxidation.

As shown in the figure, the most efficient soot oxidation is achieved on BaMnCe for which there is a match between the two T_m values within the required temperature interval of 350–450 °C. It is known from the H_2–TPR profiles that the reducibility of MnO_x–CeO_2 mixed oxides is weakened to some extent by the coverage with barium salt. Correspondingly, the thermal stability of bidentate/monodentate nitrates coordinated to Mn^{x+} and Ce^{x+} sites is slightly elevated as shown by the *in situ* DRIFT spectra. The more stable ionic nitrate $Ba(NO_3)_2$ seems to be less important for soot oxidation since its decomposition peak temperature is a little higher than 450 °C. That is the case of BaMn and BaCe on which the effect of stored nitrates on soot oxidation is greatly limited by equilibrium concentration of NO_2.

4.2. Effect of nitrate decomposition amount

The amounts of NO_x desorbed within 350–450 °C were estimated from the NO_x–TPD profiles, and are related to the maximal soot oxidation rate temperatures in Fig. 8. The activity of the catalyst seems to depend on the amount of NO_x releasable within this temperature interval, too. The relatively stable nitrate storage capacity of catalysts follows the order of BaMnCe > BaMn > MnCe > BaCe, which correlates well with the sequence of soot oxidation activity. This may account for the relatively lower activity of MnCe than the corresponding Ba–loaded catalyst in the presence of NO. It also helps to explain the much lower T_m of BaMn than BaCe although their nitrate decomposition temperatures are similar.

It should be noted that the NO_x–TPD tests were performed under N_2 while the soot–TPO tests were carried out in the presence of NO and O_2. The contribution of NO_2 produced by catalytic oxidation of NO can not be neglected especially for soot oxidation with the powerful oxidative BaMn catalyst. The situation is further complicated by the possibility for desorbed NO to be re–oxidized back to NO_2 on reactive oxygen sites. Again, the existence of carbonaceous reducing agent makes the interpretation of soot oxidation reaction further complicated. In this sense, further work needs to be done to obtain a more precise description for relationship between the readily releasable NO_x at mild temperatures and soot oxidation activity.

4.3. Role of nitrate in soot oxidation

It can be suggested based on the above observations that the nitrate decomposition within the required temperature interval (350–450 °C) is especially important for NO_x–assisted soot oxidation. These relative stable nitrates may react directly with the adjacent carbon atoms (Eq. (1)) or decompose to release NO_2 to react with soot (Eqs. (2) and (3)), accompanied by a production of NO.

$$C + M^{x+}\text{–}NO_3 \rightarrow CO_2 + NO + M^{x+}\text{–}O \quad (1)$$

$$M^{x+}\text{–}NO_3 \rightarrow M^{x+}\text{–}O + NO_2 \quad (2)$$

$$NO_2 + C \rightarrow CO_2 + NO \quad (3)$$

where M represents the metal active sites including Mn^{x+}, Ce^{x+} and Ba^{2+} cations. As discussed above, the ionic barium nitrate is less important to soot oxidation due to its higher thermal stability.

Another important issue is that the estimated value of NO_x desorbed on BaMnCe is far from the required amount of oxidant for complete combustion of soot. Fig. 9 shows the evolutions of the CO_2, O_2 and NO concentrations during the TPO test with the soot–BaMnCe mixture. It is supported by the fact that the maximal CO_2 production is about 4% while the maximal concentration of NO released is less than 5000 ppm. That is to say, the stored nitrates (and/or nitrate–derived NO_2) and NO–derived NO_2 can not meet the requirement of soot oxidation even they are fully utilized. Some heat produced locally by the reaction between soot and NO_2 can initiate the oxidation of soot by oxygen. In this sense, the nitrates and/or nitrate–derived NO_2 can be considered as a "trigger" for the extensive oxidation of soot by oxygen. In turn, the further decomposition of nitrates is accelerated by the exothermic soot oxidation reaction and hereby the thermodynamic–driven decomposition of NO_2 also contributes to the NO rise. Similar phenomena are observed on the other catalysts.

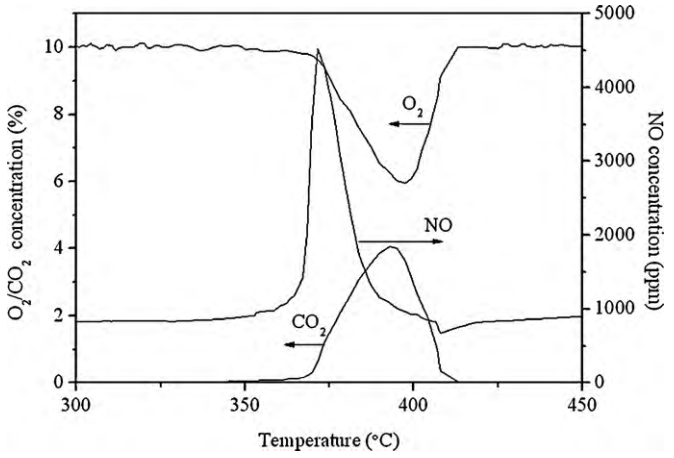

Fig. 9. Evolutions of CO_2, O_2 and NO during the soot–TPO test with the BaMnCe catalyst.

5. Conclusions

Although MnO_x–CeO_2 mixed oxides experience a certain loss in specific surface area and low–temperature reducibility after loading barium, the ternary catalyst shows a superior NO_x-assisted soot oxidation activity under an energy transference controlled regime. The amount of NO_x desorbed from BaMnCe within the temperature interval of 350–450 °C is 2.8 times of that from MnCe, which is extraordinarily important due to a match between the nitrate decomposition temperature and soot oxidation temperature with heat transfer limitations. The reaction between soot and the nitrate/nitrate–derived NO_2 is suggested to act as a "trigger" for the extensive oxidation of soot by oxygen.

Acknowledgements

The authors would like to acknowledge the National High–tech Research and Development Programs 2009AA064801, 2009AA06Z348 and National Basic Research Program of China 2010CB732304 supported by the Ministry of Science and Technology of China.

References

[1] B. Giechaskiel, B. Alföldy, Y. Drossinos, A metric for health effects studies of diesel exhaust particles, J. Aerosol Sci. 40 (2009) 639–651.
[2] M. Jeguirim, V. Tschamber, P. Ehrburger, Catalytic effect of platinum on the kinetics of carbon oxidation by NO_2 and O_2, Appl. Catal. B 76 (2007) 235–240.
[3] M. Kalogirou, D. Katsaounis, G. Koltsakis, Z. Samaras, Measurements of diesel soot oxidation kinetics in an isothermal flow reactor–catalytic effects using Pt based coatings, Top. Catal. 42–43 (2007) 247–251.
[4] Q. Li, M. Meng, Z.Q. Zou, X.G. Li, Y.Q. Zha, Simultaneous soot combustion and nitrogen oxides storage on potassium–promoted hydrotalcite–based CoMgAlO catalysts, J. Hazard. Mater. 161 (2009) 366–372.
[5] X.D. Wu, D.X. Liu, K. Li, J. Li, D. Weng, Role of CeO_2–ZrO_2 in diesel soot oxidation and thermal stability of potassium catalyst, Catal. Commun. 8 (2007) 1274–1278.
[6] D. Weng, J. Li, X.D. Wu, F. Lin, Promotional effect of potassium on soot oxidation activity and SO_2–poisoning resistance of Cu/CeO_2 catalyst, Catal. Commun. 9 (2008) 1898–1901.
[7] M.A. Peralta, M.S. Gross, B.S. Sánchez, C.A. Querini, Catalytic combustion of diesel soot: Experimental design for laboratory testing, Chem. Eng. J. 152 (2009) 234–241.
[8] M.S. Gross, M.A. Ulla, C.A. Querini, Catalytic oxidation of diesel soot: New characterization and kinetic evidence related to the reaction mechanism on K/CeO_2 catalyst, Appl. Catal. A 360 (2009) 81–88.
[9] B.S. Sánchez, C.A. Querini, E.E. Miró, NO_x adsorption and diesel soot combustion over La_2O_3 supported catalysts containing K, Rh and Pt, Appl. Catal. A 366 (2009) 166–175.
[10] A.S. Ivanova, G.S. Litvak, V.V. Mokrinskii, L.M. Plyasova, V.I. Zaikovskii, V.V. Kaichev, A.S. Noskov, The influence of the active component and support nature, gas mixture composition on physicochemical and catalytic properties of catalysts for soot oxidation, J. Mol. Catal. A 310 (2009) 101–112.
[11] K. Krishna, M. Makkee, Soot oxidation over NO_x storage catalysts: Activity and deactivation, Catal. Today 114 (2006) 48–56.
[12] L. Castoldi, Roberto Matarrese, Luca Lietti, Pio Forzatti, Simultaneous removal of NO_x and soot on Pt–Ba/Al_2O_3 NSR catalysts, Appl. Catal. B 64 (2006) 25-34.
[13] M.A. Peralta, V.G. Milt, L.M. Cornaglia, C.A. Querini, Stability of Ba,K/CeO_2 catalyst during diesel soot combustion: Effect of temperature, water, and sulfur dioxide, J. Catal. 242 (2006) 118–130.
[14] V.G. Milt, M.A. Peralta, M.A. Ulla, E.E. Miró, Soot oxidation on a catalytic NOx trap: Beneficial effect of the Ba–K interaction on the sulfated Ba,K/CeO_2 catalyst, Catal. Commun. 8 (2007) 765–769.
[15] V.G. Milt, C.A. Querini, E.E. Miró, M.A. Ulla, Abatement of diesel exhaust pollutants: NO_x adsorption on Co,Ba,K/CeO_2 catalysts, J. Catal. 220 (2003) 424–432.
[16] V.G. Milt, E.D. Banús, M.A. Ulla, E.E. Miró, Soot combustion and NO_x adsorption on Co,Ba,K/ZrO_2, Catal. Today 133–135 (2008) 435–440.
[17] E.D. Banús, V.G. Milt, E.E. Miró, M.A. Ulla, Structured catalyst for the catalytic combustion of soot: Co,Ba,K/ZrO_2 supported on Al_2O_3 foam, Appl. Catal. A 362 (2009) 129–138.
[18] L.N. Sui, L.Y. Yu, Diesel soot oxidation catalyzed by Co–Ba–K catalysts: Evaluation of the performance of the catalysts, Chem. Eng. J. 142 (2008) 327–330.
[19] K. Tikhomirov, O. Kröcher, M. Elsener, A. Wokaun, MnO_x–CeO_2 mixed oxides for the low–temperature oxidation of diesel soot, Appl. Catal. B 64 (2006) 72–78.
[20] K. Ito, K. Kishikawa, A. Watajima, K. Ikeue, M. Machida, Soot combustion activity of NO_x–sorbing Cs–MnO_x–CeO_2 catalysts, Catal. Commun. 8 (2007) 2176–2180.
[21] G.A. Merkel, W.A. Cutler, C.J. Warren, Thermal durability of wall–flow ceramic diesel particulate filters, SAE Paper No. 2001-01-0190.
[22] G. Kolios, A. Gritsch, A. Morillo, U. Tuttlies, J. Bernnat, F. Opferkuch, G. Eigenberger, Heat–integrated reactor concepts for catalytic reforming and automotive exhaust purification, Appl. Catal. B 70 (2007) 16–30.
[23] M.A. Peralta, M.S. Gross, M.A. Ulla, C.A. Querini, Catalyst formulation to avoid reaction runaway during diesel soot combustion, Appl. Catal. A 367 (2009) 59–69.
[24] I.C.L. Leocadio, C.V. Miñana, S. Braun, M. Schmal, Effect of experimental conditions on the parameters used for evaluating the performance of the catalyst Mo/Al_2O_3 in diesel soot combustion, Appl. Catal. B 84 (2008) 843–849.
[25] Q. Liang, X.D. Wu, D. Weng, H.B. Xu, Oxygen activation on Cu/Mn–Ce mixed oxides and the role in diesel soot oxidation, Catal. Today 139 (2008) 113–118.
[26] J. Trawczyński, B. Bielak, W. Mišta, Oxidation of ethanol over supported manganese catalysts–effect of the carrier, Appl. Catal. B 55 (2005) 277–285.
[27] K.I. Hadjiivanov, Identification of neutral and charged N_xO_y surface species by IR spectroscopy, Catal. Rev. 42 (2000) 71–144.
[28] X.D. Wu, Q. Liang, D. Weng, Z.X. Lu, The catalytic activity of CuO–CeO_2 mixed oxides for diesel soot oxidation with a NO/O_2 mixture, Catal. Commun. 8 (2007) 2110–2114.
[29] I. Atribak, B. Azambre, A. Bueno López, A. García–García, Effect of NO_x adsorption/desorption over ceria–zirconia catalysts on the catalytic combustion of model soot, Appl. Catal. B 92 (2009) 126–137.
[30] A.L. Kustov, M. Makkee, Application of NO_x storage/release materials based on alkali–earth oxides supported on Al_2O_3 for high–temperature diesel soot oxidation, Appl. Catal. B 88 (2009) 263–271.